Atomically-thin Single-photon Sources for Quantum Communication - Supplementary

Timm Gao,[1] Martin v. Helversen,[1] Carlos Anton-Solanas,[2,3] Christian Schneider,[2] and Tobias Heindel[1,*]

[1] *Institut für Festkörperphysik, Technische Universität Berlin, 10623 Berlin, Germany*
[2] *Institut für Physik, Carl von Ossietzky Universität Oldenburg, 26111 Oldenburg, Germany*
[3] *Current address: Departamento de Física de Materiales, Instituto Nicolás Cabrera, and Instituto de Física de la Materia Condensada, Universidad Autónoma de Madrid, 28049 Madrid, Spain*

PHOTON ARRIVAL TIME DISTRIBUTIONS

For investigating the performance of the receiver module, the receiver's response to all four possible input polarization states is investigated. We sequentially prepare single photon pulses in horizontal (H), vertical (V), diagonal (D), and anti-diagonal (A) polarization. The events are detected at all four detectors and individually correlated with the laser synchronization signal to obtain time-resolved measurements. These are summarized in Supplementary Figure 1 on the left-hand side in a 4x4 matrix. The rows correspond to the input polarization and the column to the respective detection channel. Histograms within one row are normalized to the maximum of the input polarization (e.g., the first row is normalized to the maximum of the HH distribution (blue)). The matrix in the main text Figure 2 b is calculated from the sum of each unnormalized matrix element in Supplementary Figure 1 divided by the acquisition time. Erroneous detection events can be made visible if the time-resolved measurement is renormalized to the arrival time probability distribution for both output channels in each basis, as depicted in the right panel of Supplementary Figure 1.

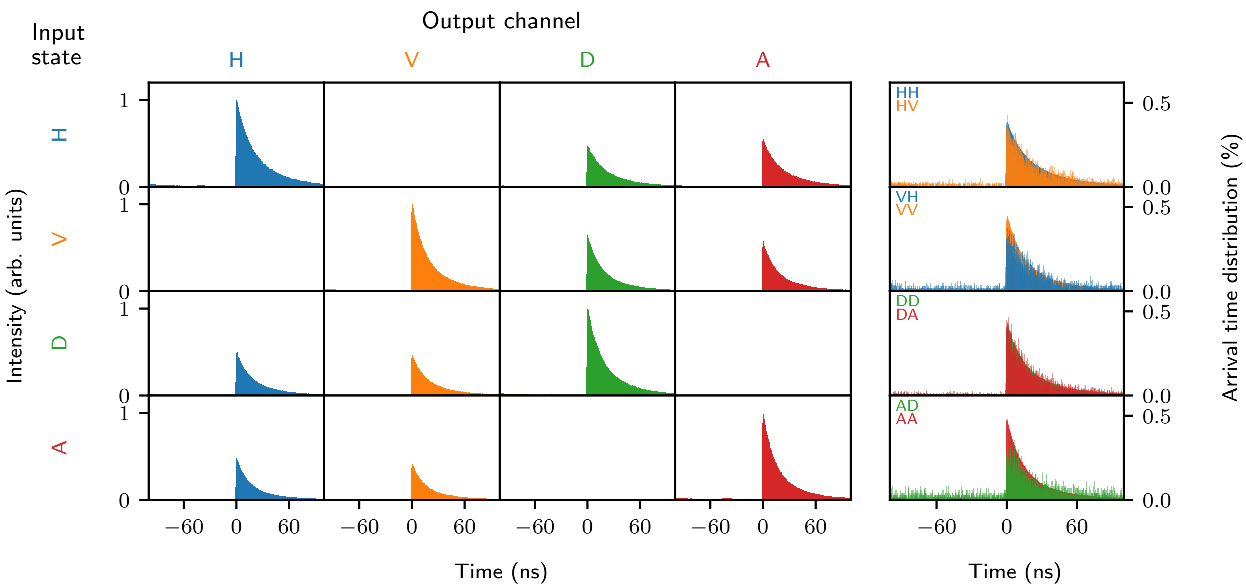

Supplementary Figure 1. Photon arrival time distributions measured at the receiver module. For each of the four possible input polarizations H, V, D, and A, the time resolved photoluminescence is measured at each of the four corresponding output channels of the receiver module individually. The time-bin width is 0.1 ns. The measurement data in the left 4x4 matrix is normalized to the maximum of the respective input state. The right panel shows the two data sets for a given input polarization basis (e.g., HH and HV). Here, each distribution is normalized to the sum of all events registered in the respective channel (e.g., the HV distribution is normalized by all clicks registered in the V-channel).

EFFECTS OF DYNAMIC STATE PREPARATION

Our study demonstrates the feasability of quantum communication using single-photon sources based on 2D-TMDCs by using a QKD testbed with static polarization-state preparation. In full implementations, effects arising from a

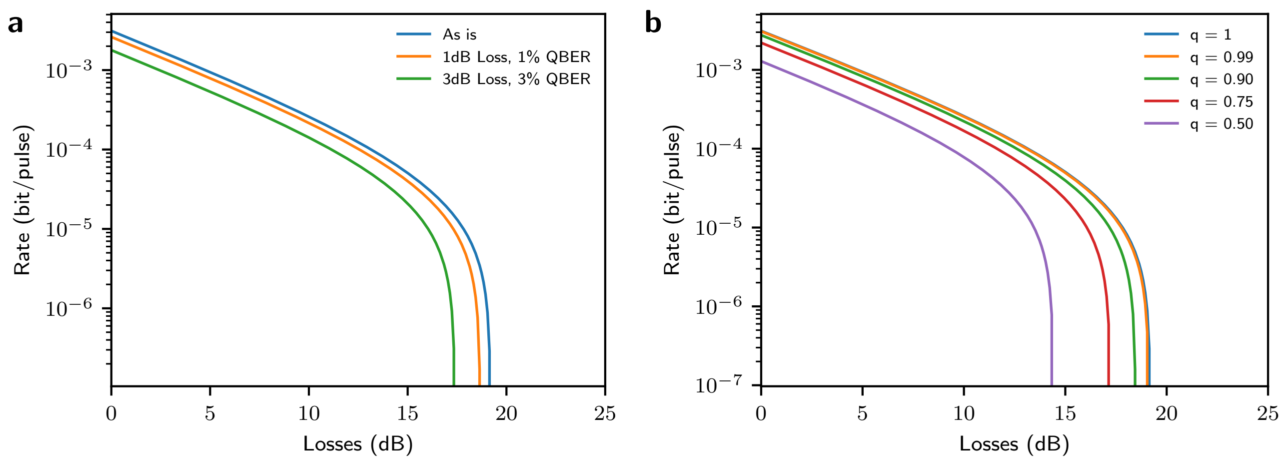

Supplementary Figure 2. Impact of dynamic state preparation on the secret key rate vs. loss in full implementations of QKD. **a** Comparison of the original data show in the main text ('As is' refers to the non-optimized case) and two realistic scenarios assuming dynamic encoding via an EOM introducing additional losses, i.e. reduced μ, and increased QBER. **b** Impact of a finite state preparation qualities q.

dynamic state preparation need to be considered in the performance and security analysis. Unlike WCP systems, however, the additional losses introduced by active modulation components like electro-optical modulators (EOMs) affect the achievable mean-photon number in the quantum channel. To gain a quantitative understanding, we consider two realistic scenarios assuming dynamic polarization-state preparation via free-space and fiber-based EOMs with typical transmission losses of 1 dB and 3 dB, respectively. The additional error EOMs contribute to the overal QBER (due to a finite extinction ratio) is typically in the range of 1 % to 3 %. Here, we assume the best case (1 dB loss, additional QBER 1 %) and the worst case (3 dB loss, additional QBER 3 %) scenarios for comparison. Supplementary Figure 2 (a) compares the simulated rate-loss dependencies for both scenarios in comparison with the original data from our WSe_2 single-photon source (without temporal filtering) based on the parameters in Table I of the main text. We find that the dynamic state preparation via EOMs noticeably affects the achievable secret key rate and tolerable loss, although the impact is moderate. Another effect resulting from dynamic encoding is a finite state preparation fidelity or quality. While this effect was negligible in our proof-of-principle experiment using a crystal polarizer with high extinction ratio, the non-ideal state preparation will result in an additional contribution to the overall QBER in full implementations. In Supplementary Figure 2 b we investigated the effect of lower state preparation fidelity using the modified key rate equation from ref. [1]:

$$S_\infty = S_{\text{sift}}\left[A\left(q - h\left(e/A\right)\right) - f_{\text{EC}} h\left(e\right)\right], \tag{1}$$

where q denotes the state preparation quality. A high fidelity of 90 % is desirable in full implementations for not loosing rate and tolerable losses.

TEMPORAL FILTERING

In our study we exploit temporal filtering on the receiver side to optimize the achievable secret key rate and tolerable losses. For this purpose, an optimal trade-off between sifted key material and QBER is required. Supplementary Figure 3 depicts the QBER and the sifted fraction for each detection channel in our four-state polarization analyzer as a function of the width Δt of the acceptance time window ($t_\text{c} = 0$). The plots are calculated from the experimental data in Supplementary Figure 1. Reducing Δt, both the QBER and the sifted key fraction is reduced. The minimal QBER achieved is limited by optical imperfections in the experimental setup, as detector noise is effectively filtered by the acceptance time window. The temporal filtering does however not only affect the sifted key fraction and QBER, but also the $g^{(2)}(0)$. While in QKD one cannot benefit from temporal filtering of $g^{(2)}(0)$ without adding modifications to the protocol implementation (see main text for details), we make use of it to estimate contributions limiting the single-photon purity of our source. Supplementary Figure 4 a shows the $g^{(2)}(0)$ of our WSe_2 single-photon source as a function of the acceptance time window Δt and t_c. For this we used a subset of the experimental data (corresponding to the first 15 min) from the measurement presented in Figure 2 d of the main text. For regions in

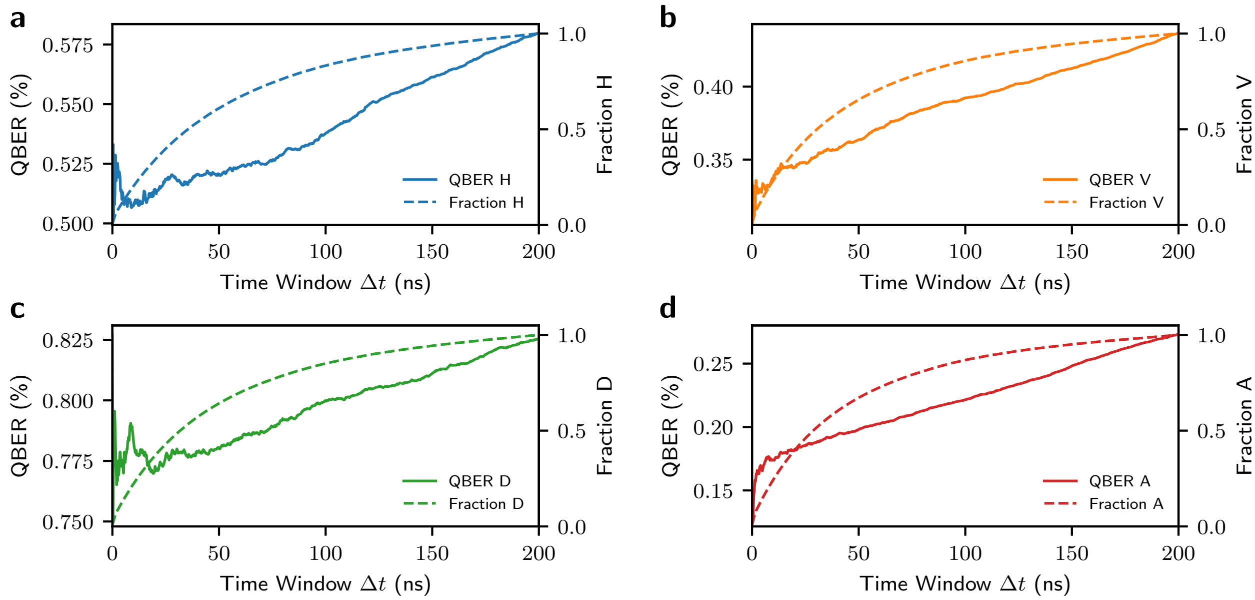

Supplementary Figure 3. Temporal filtering with fixed $t_c = 0$. **a** H input polarization. **b** V input polarization. **c** D input polarization. **d** A input polarization. From the photon arrival time distributions in Supplementary Figure 1 the QBERs and corresponding fractions of the sifted key are calculated depending on the width of the acceptance time window.

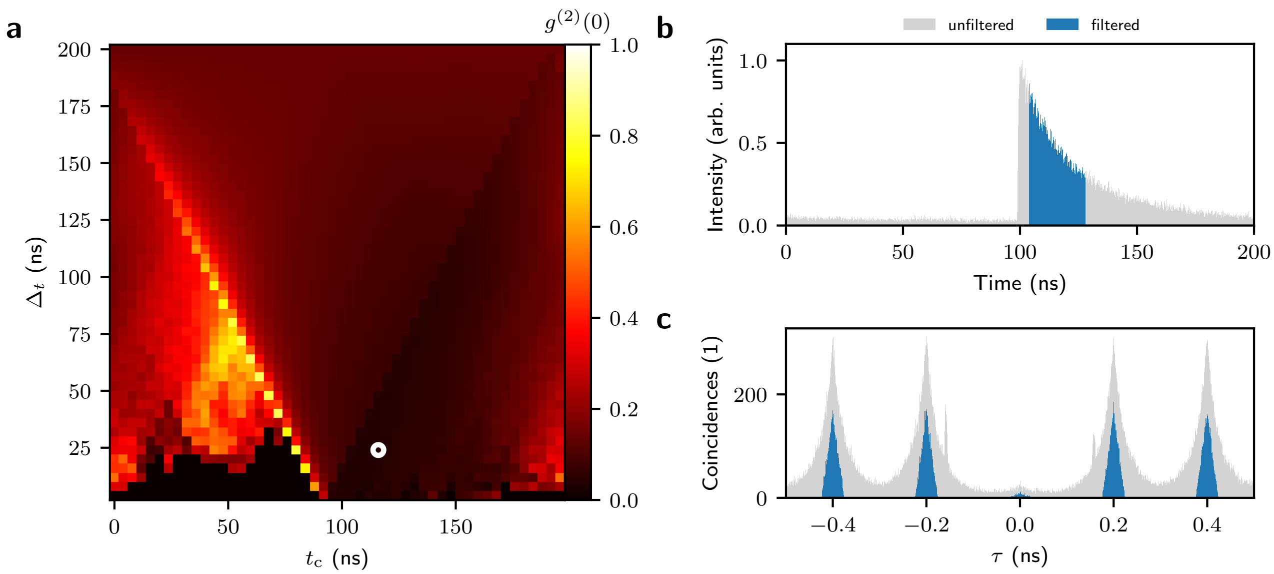

Supplementary Figure 4. 2D Temporal filtering of $g^{(2)}(0)$. **a** $g^{(2)}(0)$ as a function of the acceptance time window Δt and t_c. The $g^{(2)}(0) = 0.034 \pm 0.002$ from the main text is marked with a white circle ($\Delta t = 24\,\text{ns}$, $t_c = 16\,\text{ns}$). **b** and **c** Photon arrival time distributions and autocorrelation histograms for the unfiltered (grey) and filtered (blue) case corresponding to the parameter set marked in **a**.

black, i.e. zero, no reasonable $g^{(2)}(0)$ could be evaluated due to insufficient statistics. The minimum $g^{(2)}(0)$ is reached in the lower right quadrant of the 2D heatmap. In this region, signal from the exponential decay of the photon arrival time distribution of the quantum emitter is predominantly accepted, while residual background contributions of laser (left half, corresponds to rising edge of the photon arrival time distribution) and a large fraction of dark count contributions (lower left quadrant) is rejected. The white circle marks the value of $g^{(2)}(0) = 0.034 \pm 0.002$ at $\Delta t = 24\,\text{ns}$, $t_c = 16\,\text{ns}$ we state in the main text, being in good agreement with our estimate on the spectral background of 0.04 caused by uncorrelated background emission of the sample. This setting of the temporal filter

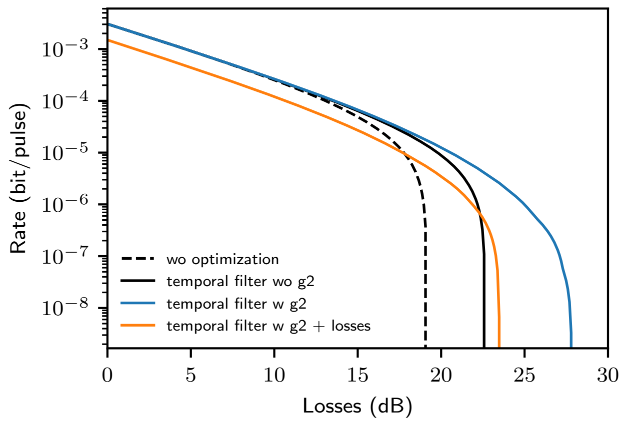

Supplementary Figure 5. Impact of 2D temporal filtering of $g^{(2)}(0)$ on the secret key rate. The gain in tolerable loss compared to the original data from the main text (full and dashed black lines, with (w) and without (wo) temporal filtering, respectively) is only significant if additional losses of an EOM are neglected (blue line). In a more realistic scenario the additional 3 dB loss of the modulator, required for active modulation on Alice's side, overcompensates the gain for our specific system (orange line).

results in a reasonable trade-off between the sifted key fraction (47 %) and the reduction of $g^{(2)}(0)$ from the unfiltered $g^{(2)}(0) = 0.139 \pm 0.002$. The photon arrival time distributions and corresponding autocorrelation histograms are shown in in Supplementary Figure 4 b and Supplementary Figure 4 c for the unfiltered (blue) and filtered (grey) case, respectively. While even lower $g^{(2)}(0)$ values can be achieved, tighter filtering leads to substantially reduced sifted key fractions. Comparing the two autocorrelation histograms in Supplementary Figure 4 c, also reveals that there is a significant difference between correlating the filtered detection events instead of using a linear background subtraction and only a certain interval around each peak of the unfiltered histogram for evaluating $g^{(2)}(0)$. For completeness, we also investigated how temporal filtering of $g^{(2)}(0)$ would affect the rate-loss dependencies in implementations with protocol extensions guaranteeing overall security, e.g. via active temporal filtering also on Alice side. Supplementary Figure 5 compares the original data from the main text (full and dashed black lines, with (w) and without (wo) temporal filtering, respectively) with cases where the reduced $g^{(2)}(0)$ due to temporal filtering is taken into account (orange and blue lines). The comparison reveals a significant gain in tolerable loss only if additional losses of an EOM are neglected (blue line). Assuming 3 dB of additional loss, the secret key rate is reduced while the tolerable loss becomes comparable to the optimized case without $g^{(2)}(0)$-filtering again. We assume 3 dB loss of the modulator as the extinction ratio of fast fiber-based EOMs is typically higher ($\approx 1:10^4$) compared to the extinction ratio possible with free-space modulators ($\approx 1:10^2$). All solid lines result from an individual 2D optimization for each loss.

REAL-TIME PHOTON STATISTICS MONITORING

For the real-time monitoring of the photon statistics, reasonable accumulation times need to be evaluated. In Figure 2 d of the main text, we choose 10 s and 100 s. The choice of these accumulation times is based on Supplementary Figure 6 depicting the antibunching $g^{(2)}(0)$ of our WSe_2 single-photon source as a function of the accumulation time. Here, the $g^{(2)}(0)$-value for accumulation times below 103 s is slightly lower even within the uncertainty bounds compared to the full measurement. This shows that a shorter acquisition time is suitable for taking changes in the emitter statistics into account. For 10 s accumulation time (0.178 Mbit sifted block size), the relative error is about 10 %, while an increase to 100 s (1.792 Mbit sifted block size) reduces the relative error below 5 %.

* Corresponding author: tobias.heindel@tu-berlin.de

[1] Tomamichel, M., Lim, C. C. W., Gisin, N. & Renner, R. Tight finite-key analysis for quantum cryptography. *Nat. Commun.* **3**, 634 (2012).

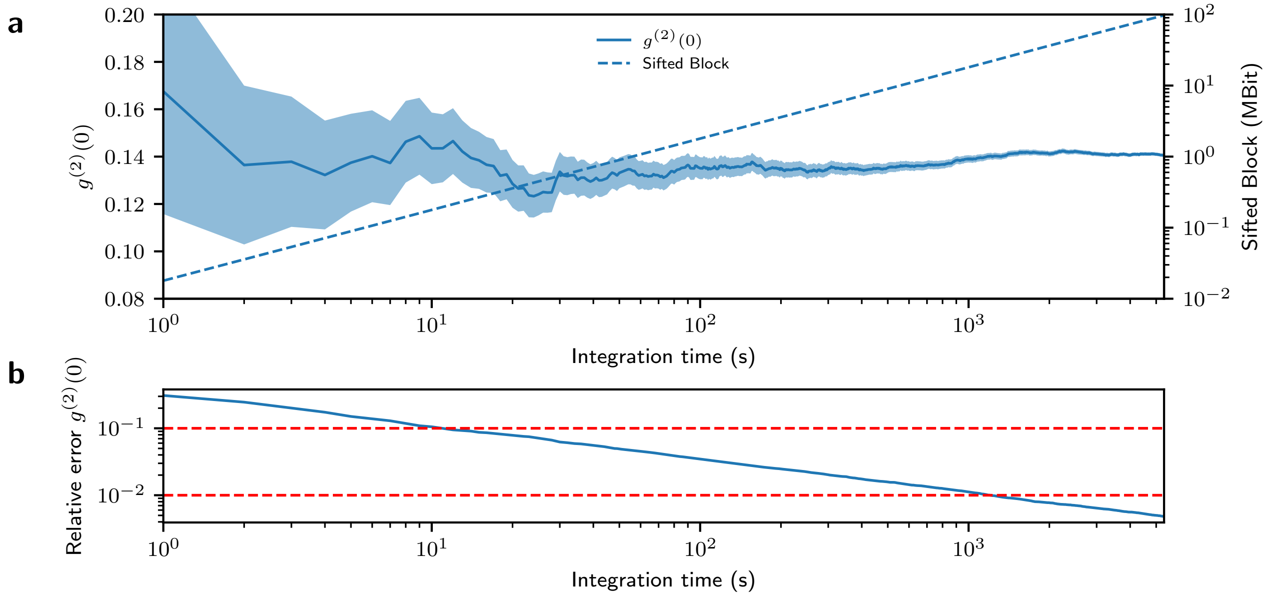

Supplementary Figure 6. Antibunching investigation over integration time. **a** The antibunching $g^{(2)}(0)$ of the SPS is evaluated via correlating the detection events of all for detectors in overlapping blocks for different accumulation times compared with the corresponding length of the sifted block. Here, the same dataset as in Figure 2 d of the main text is used. **b** Relative error of $g^{(2)}(0)$ over the integration time.